2018 IEEE-RAS 18th International Conference on Humanoid Robots (Humanoids)
Beijing, China, November 6-9, 2018

Joint Force Analysis and Moment Efficiency Index of Cable-Driven Rehabilitation Devices

Hao Xiong, Lin Zhang, Zhongyuan Liu, and Xiumin Diao, *Member, IEEE*

***Abstract*—Cable-driven rehabilitation devices (CDRDs) have been studied by many researchers in the past decade. While a CDRD rotates a human joint by generating an assistant moment about the axis of the joint, it also creates a resultant force acting on the joint as long as the assistant moment is nonzero. Such a joint force may cause excessive joint wear or even break the joint if it exceeds a threshold. Thus, it is critical to analyze not only the assistant moment generated by a CDRD to rotate the joint, but also the joint force to have a safe and effective rehabilitation training. This paper studies how a CDRD with three degrees of freedom (DOFs) and four cables exerts a joint force on a general three-DOF human joint. The kinematics and dynamics models of the CDRD are established and the joint force needed to provide the assistant moment is derived mathematically at first. Then, an index to evaluate the efficiency of a CDRD in providing assistant moment (i.e., moment efficiency) is proposed. Lastly, a case study of the flexion and extension of the knee assisted by a CDRD is presented to demonstrate the derivation of the joint force and the usage of the moment efficiency index. The moment efficiency index not only promotes the safety of rehabilitation training, but also provides a guideline for the design of CDRDs.**

Keywords — joint force, moment efficiency index, cable-driven rehabilitation device, wearable device

I. Introduction

Stroke is a comparative cause of permanent disability and severe impairments often come with survivors of stroke [1]. The main symptoms of survivors with impairments are loss of muscle strength, spasticity, and lack of coordination of muscle activation [2]. These lost capabilities are necessary to perform basic activities of daily living. Thus, impairments significantly reduce a survivor's quality of life [3]. Rehabilitation devices with various power-transmission approaches have been proven effective and efficient in helping trainees restore their lost capabilities [4]. Compared with power-transmission approaches such as gear transmission, belt transmission, and ball-screw transmission [5], transmitting power using cables or wires provides a rehabilitation device with many merits, such as low inertia, high payload-to-weight ratio, modularity, and reconfiguration [6], [7]. Therefore, several cable-driven rehabilitation devices (CDRDs) have been proposed in the past decade [8]–[16]. An example CDRD for the knee and the ankle is shown in Fig. 1.

Fig. 1. An example CDRD for the knee and the ankle

There are usually two categories of interfaces between a CDRD and a trainee, namely, rigid cuff and soft brace. Cable-driven exoskeletons with metal cuffs were developed for upper limb rehabilitation [8], [9] and lower limb rehabilitation [10], respectively. Chen et al. [12] demonstrated a cable-driven exoskeleton with metal cuffs for wrist rehabilitation. A cable-driven robotic device was also proposed in [11] for ankle rehabilitation. Moreover, soft braces were employed in CDRDs for shoulder rehabilitation [13] [14], knee assistance [15], and ankle assistance [16].

To gain the mobility of a human joint, a CDRD usually rotates the joint repeatedly by generating an assistant moment about the axis of the joint [17]. In order to generate such an assistant moment during rehabilitation training, the CDRD needs to exert a force on the joint. Such a force may cause excessive wear of the joint or even break the joint if it exceeds a threshold. Thus, it is critical to analyze not only the assistant moment generated by the CDRD to rotate the joint, but also the joint force exerted by the CDRD on the joint for the sake of safety and the design of CDRDs. Joint force issues have been discussed by a few researchers in the study of human-robot interaction for rehabilitation training. A method of trajectory optimization was proposed for a cable-driven upper arm exoskeleton to minimize the assistant moment and joint force in [18]. A method of evaluating whether a joint force is

H. Xiong is with the School of Engineering Technology, Purdue University, West Lafayette, IN 47907 USA (e-mail: xiong60@purdue.edu).
L. Zhang is with the School of Engineering Technology, Purdue University, West Lafayette, IN 47907 USA (e-mail: zhan2838@purdue.edu).
Z. Liu is with the School of Mechanical Engineering, Shanghai Jiao Tong University, Shanghai, China 200240 (e-mail: lallal@sjtu.edu.cn)
X. Diao is with the School of Engineering Technology, Purdue University, West Lafayette, IN 47907 USA (corresponding author: phone: 765-494-2212; fax: 765-494-6219; e-mail: diaox@purdue.edu).

safe was presented for human-care robots in [19]. The threshold of a safe joint force is defined in [19] as the minimal force that can cause injury to a human joint. However, a general analysis of the joint force generated by a CDRD is still not available in the literature. Such a joint fore analysis can help evaluate the efficiency of the CDRD in providing assistant moment (called moment efficiency in this paper) with respect to generated joint force.

This paper presents a general analysis of the joint force generated by a CDRD, assuming that there is no collision between cables and the human body, and proposes a moment efficiency index to evaluate the moment efficiency of the CDRD. The rest of the paper is organized as follows. Section II proposes the kinematics and dynamics models of a general three-DOF human joint assisted by a CDRD. In section III, a moment efficiency index is proposed. A joint force analysis of the knee with one degree of freedom (DOF) assisted by a CDRD with four cables is conducted in section IV. Finally, Section V summarizes this paper.

II. Modeling of Kinematics and Dynamics

In this section, the kinematics and dynamics of a general three-DOF human joint assisted by a three-DOF CDRD with four cables are presented. A three-DOF CDRD with four cables can be fully-constrain [20] and thus, it can assist all three DOFs of the joint.

A. Kinematics Analysis

The kinematics architecture of a general three-DOF human joint (in aqua) assisted by a three-DOF CDRD (in red) with four cables is shown in Fig. 2. A_i and B_i are the two attaching points of the ith cable on the base and the end-effector, respectively. The base and the end-effector are worn on the two parts of the joint, respectively. $\boldsymbol{l}_i \in R^3\ (i = 1,2,3,4)$ is the vector along the ith cable. $\boldsymbol{u}_i$ is the unit vector along the ith cable. The magnitude of vector $\boldsymbol{l}_i$, represented by scalar l_i, is the length of the ith cable between attaching points A_i and B_i. The positions of the attaching points A_i and $B_i$are represented by vectors $\boldsymbol{a}_i$ and $\boldsymbol{b}_i$, respectively. Obviously, $\boldsymbol{a}_i$ is a constant vector in the base frame F_b and $\boldsymbol{b}_i$ is a constant vector in the end-effector frame F_e. The origin of the base frame is denoted by point O, and the origin of the end-effector frame F_e is denoted as point P. Both O and P locate at the rotation center of the end-effector, namely the rotation center of the joint. The attitude of F_e with respect to F_b is described by three Euler angles $\boldsymbol{\Omega} = [\psi, \theta, \phi]^T$ with the Z-Y-X sequence.

Based on the above kinematics notations, the position of the end-effector with respect to the based frame can be described as [21]

$$\boldsymbol{p} = \boldsymbol{a}_i - \boldsymbol{l}_i - \boldsymbol{b}_i \quad for\ i = 1,2,3,4 \tag{1}$$

from which one has

$$l_i^2 = [\boldsymbol{a}_i - \boldsymbol{p} - \boldsymbol{b}_i]^T[\boldsymbol{a}_i - \boldsymbol{p} - \boldsymbol{b}_i] \quad for\ i = 1,2,3,4 \tag{2}$$

Differentiating (2) with respect to time, and then organizing the four resulting equations into a matrix form, one obtains

$$\dot{\boldsymbol{l}} = \boldsymbol{J}\dot{\boldsymbol{X}} \tag{3}$$

where

$$\dot{\boldsymbol{l}} = [\dot{l}_1\ \dot{l}_2\ \dot{l}_3\ \dot{l}_4]^T \tag{4}$$

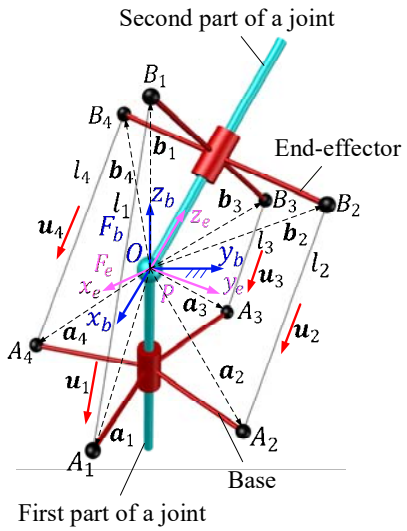

Fig. 2. Kinematics notations of a general three-DOF human joint (in aqua) assisted by a three-DOF four-cable CDRD (in red)

$$\boldsymbol{J} = \begin{bmatrix} \boldsymbol{u}_1 & \boldsymbol{u}_2 & \boldsymbol{u}_3 & \boldsymbol{u}_4 \\ \boldsymbol{b}_1 \times \boldsymbol{u}_1 & \boldsymbol{b}_2 \times \boldsymbol{u}_2 & \boldsymbol{b}_3 \times \boldsymbol{u}_3 & \boldsymbol{b}_4 \times \boldsymbol{u}_4 \end{bmatrix}^T \tag{5}$$

$$\dot{\boldsymbol{X}} = \begin{bmatrix} \boldsymbol{v} \\ \boldsymbol{\omega} \end{bmatrix} = [\dot{x}\ \dot{y}\ \dot{z}\ \dot{\theta}_x\ \dot{\theta}_y\ \dot{\theta}_z]^T \tag{6}$$

In the above equations, $\dot{\boldsymbol{l}}$ is the velocity vector in the joint space. $\dot{\boldsymbol{X}}$ denotes the twist of the end-effector. $\boldsymbol{v} = [\dot{x}\ \dot{y}\ \dot{z}]^T$ and $\boldsymbol{\omega} = [\dot{\theta}_x\ \dot{\theta}_y\ \dot{\theta}_z]^T$ represent the translational and rotational velocity vectors of F_b with respect to F_e. $\boldsymbol{J}$ is the Jacobian matrix of the CDRD.

The rotation matrix transforming a vector from F_e to F_b is [22]–[25]

$$\boldsymbol{R}_e^b = \begin{bmatrix} C_\psi C_\theta & C_\psi S_\theta S_\phi - S_\psi C_\phi & C_\psi S_\theta C_\phi + S_\psi S_\phi \\ S_\psi C_\theta & S_\psi S_\theta S_\phi + C_\psi C_\phi & S_\psi S_\theta C_\phi - C_\psi S_\phi \\ -S_\theta & C_\theta S_\phi & C_\theta C_\phi \end{bmatrix} \tag{7}$$

where C_{angle} and S_{angle} are designated as $\cos(angle)$ and $\sin(angle)$, respectively. $\boldsymbol{R}_e^b$ is orthogonal, so the rotation matrix transforming a vector from F_b to F_e is [22]–[25]

$$\boldsymbol{R}_b^e = [\boldsymbol{R}_e^b]^{-1} = [\boldsymbol{R}_e^b]^T \tag{8}$$

The rotation matrix transforming the angular velocity of the end-effector from F_e to F_b is [22]–[25]

$$\boldsymbol{R}_\omega^\Omega = \begin{bmatrix} 1 & S_\phi T_\theta & C_\phi T_\theta \\ 0 & C_\phi & -S_\phi \\ 0 & S_\phi / C_\theta & C_\phi / C_\theta \end{bmatrix} \tag{9}$$

where T_{angle} is designated as $\tan(angle)$. To convert angular velocity of the end-effector from F_e to F_b, one has

$$\dot{\boldsymbol{\Omega}} = \boldsymbol{R}_\omega^\Omega \boldsymbol{\omega} \tag{10}$$

where $\dot{\boldsymbol{\Omega}}$ is the angular velocity of the end-effector in F_b. The rotation matrix transforming the angular velocity of the end-effector from F_b to F_e is [22]–[25]

$$\boldsymbol{R}_\Omega^\omega = \begin{bmatrix} 1 & 0 & -S_\theta \\ 0 & C_\phi & C_\theta S_\phi \\ 0 & -S_\phi & C_\theta C_\phi \end{bmatrix} \tag{11}$$

B. Dynamics Analysis

Compared to the inertia of the end-effector, the inertia of cables is usually much smaller and can be ignored [26]. Then, the motion of the end-effector can be expressed based on Newton-Euler Formulation with respect to the end-effector frame F_e as,

$$\boldsymbol{M}(\boldsymbol{X})\ddot{\boldsymbol{X}} + \boldsymbol{C}(\boldsymbol{X},\dot{\boldsymbol{X}})\dot{\boldsymbol{X}} + \boldsymbol{G}(\boldsymbol{X}) + \boldsymbol{F}_j(\boldsymbol{X}) = -\boldsymbol{J}^T\boldsymbol{\tau} \quad (12)$$

where $\boldsymbol{M}(\boldsymbol{X})$ denotes the mass matrix. $\boldsymbol{C}(\boldsymbol{X},\dot{\boldsymbol{X}})$ denotes the Coriolis and centripetal matrix. $\boldsymbol{G}(\boldsymbol{X})$ represents the 6×1 gravity vector. $\boldsymbol{F}_j(\boldsymbol{X})$ represents the 6×1 joint wrench vector. The mass matrix $\boldsymbol{M}(\boldsymbol{X})$, Coriolis and centripetal matrix $\boldsymbol{C}(\boldsymbol{X},\dot{\boldsymbol{X}})$, and the gravity matrix $\boldsymbol{G}(\boldsymbol{X})$ in (12) have been defined by several scholars [27], [28]

$$\boldsymbol{M}(\boldsymbol{X}) = \begin{bmatrix} m\boldsymbol{I}_{3\times3} & \boldsymbol{0}_{3\times3} \\ \boldsymbol{0}_{3\times3} & \boldsymbol{I}_p \end{bmatrix} \quad (13)$$

$$\boldsymbol{C}(\boldsymbol{X},\dot{\boldsymbol{X}})\dot{\boldsymbol{X}} = \begin{bmatrix} \boldsymbol{\omega} \times m\boldsymbol{v}_p \\ \boldsymbol{\omega} \times \boldsymbol{I}_p\boldsymbol{\omega} \end{bmatrix} \quad (14)$$

$$\boldsymbol{G}(\boldsymbol{X}) = \begin{bmatrix} \boldsymbol{F}_g \\ \boldsymbol{W}_g \end{bmatrix} \quad (15)$$

$$\boldsymbol{F}_j(\boldsymbol{X}) = \begin{bmatrix} \boldsymbol{F}_j \\ \boldsymbol{0}_{3\times1} \end{bmatrix} \quad (16)$$

where $\boldsymbol{v}_p$ is the translational velocity vector of the center of mass of the end-effector in F_e. $\boldsymbol{I}_p$ is the inertia tensor of the end-effector about point P in F_e. $\boldsymbol{I}_{3\times3}$ is the 3×3 identity matrix. $\boldsymbol{0}_{3\times3}$ is the 3×3 zero matrix. $\boldsymbol{0}_{3\times1}$ is the 3×1 zero vector. $\boldsymbol{F}_g$ is the gravity of the end-effector in F_e, and $\boldsymbol{W}_g$ is the moment of the gravity about point P in F_e. $\boldsymbol{F}_j$ is the 3×1 joint force exerted on the joint by the end-effector. Moreover, one can write $\boldsymbol{J}^T\boldsymbol{\tau}$ as

$$\boldsymbol{J}^T\boldsymbol{\tau} = \begin{bmatrix} \boldsymbol{F}_t \\ \boldsymbol{W}_t \end{bmatrix} \quad (17)$$

where $\boldsymbol{F}_t$ is the resultant force of the cable tensions in F_e, and $\boldsymbol{W}_t$ is the resultant moment of the cable tensions about point P in F_e.

Since the joint has three rotational DOFs, and the origin of the end-effector frame and the base frame are both set at the rotation center of the joint, one has $\dot{\boldsymbol{X}} = \begin{bmatrix} 0 & 0 & 0 & \dot{\theta}_x & \dot{\theta}_y & \dot{\theta}_z \end{bmatrix}^T$ and $\ddot{\boldsymbol{X}} = \begin{bmatrix} 0 & 0 & 0 & \ddot{\theta}_x & \ddot{\theta}_y & \ddot{\theta}_z \end{bmatrix}^T$. Then the last three equations of (12) can be rewritten as

$$\boldsymbol{I}_p\dot{\boldsymbol{\omega}} + \boldsymbol{\omega} \times \boldsymbol{I}_p\boldsymbol{\omega} + \boldsymbol{W}_g = -\boldsymbol{W}_t \quad (18)$$

where $\dot{\boldsymbol{\omega}}$ is the derivative of $\boldsymbol{\omega}$. The first three equations of (12) can be rewritten as

$$\boldsymbol{F}_j = -\boldsymbol{F}_t - \boldsymbol{F}_g - \boldsymbol{\omega} \times m\boldsymbol{v}_p \quad (19)$$

where (18) determines the rotation of the end-effector, and the joint force can be calculated based on (19).

III. Moment Efficiency Index of a CDRD

According to (15), (17), and (19), the joint force generated by the CDRD is $-\boldsymbol{F}_t$ and the joint force generated by the gravity of the end-effector is $-\boldsymbol{F}_g$. Moreover, the joint force generated by the centrifugal is $-\boldsymbol{\omega} \times m\boldsymbol{v}_p$. This paper defines a moment efficiency index η as the magnitude of the assistant moment of the CDRD (i.e., $|\boldsymbol{W}_t|$) divided by the magnitude of the joint force generated by the CDRD (i.e., $|\boldsymbol{F}_t|$)

$$\eta = \frac{|\boldsymbol{W}_t|}{|\boldsymbol{F}_t|} \quad (20)$$

The characteristic length of η is set to 1 m in this study, so the unit of η is homogeneous [29]. The moment efficiency index reflects the ability of a CDRD to assist a joint while leading to a unit magnitude of joint force acting on the joint. η varies according to the orientation of the joint and the design of the CDRD.

Antagonistic cable tensions [30], [31] of a CDRD are cable tensions that balance each other. Since a joint with three rotational DOFs can balance any translational force in theory, antagonistic cable tension vector of the CDRD with three rotational DOFs, noted as $\boldsymbol{\tau}_a$, satisfies

$$\boldsymbol{J}^T\boldsymbol{\tau}_a = \begin{bmatrix} \boldsymbol{F}_a \\ \boldsymbol{0}_{3\times1} \end{bmatrix} \quad (21)$$

In this case, antagonistic cable tensions only balance the moment generated by each other. The resultant force generated by antagonistic cable tensions acts on the joint. It should be noted from (21) that, since antagonistic cable tensions create zero moment, they do not affect the rotation of the end-effector. However, antagonistic cable tensions do create a nonzero joint force, denoted as $\boldsymbol{F}_a$, acting on the joint. According to (21), in the force-closure workspace [21] of the CDRD, increasing antagonistic cable tensions does not affect the wrench acting on the end-effector, but it does increase the magnitude of the joint force generated by the CDRD. Thus, based on (20), the moment efficiency index will decrease.

IV. A Knee Assisted by a CDRD with Four Cables

In this section, a knee with one DOF (i.e., flexion and extension) assisted by an example three-DOF four-cable CDRD, as shown in Fig. 3, is discussed based on the moment efficiency index in quasi-static conditions. The collision between cables, cuffs, the shank, and the upper leg are not taken into account in this discussion. One cuff with a radius of 0.1 m is worn on the upper leg and the shank, respectively. The shank is able to rotate about x_e axis. The angle of the knee, denoted as ϕ_k, is measured from the shank to z_b axis. Let d_u denote the distance between the centroid of the cuff worn on the upper leg and the knee joint. Let d_s denote the distance between the centroid of the cuff worn on the shank and the knee joint. Both d_u and d_s are variables in this study. Initially, F_e coincides with F_b, and the positions of the anchor points are shown in TABLE I.

According to (20) and (21), if the angle of the knee, the position of the upper leg cuff, and the position of the shank cuff are given, the maximum moment efficiency index, denoted by η_{max}, is achieved when the antagonistic cable tensions are all zero. In the simulation, the maximum moment efficiency index is calculated in the force-closure workspace of the CDRD. The maximum moment efficiency of the CDRD with respect to d_s and d_u in assisting the flexion and extension of the knee are plotted in Figs. 4 and 5, respectively.

According to Figs. 4 and 5, the angle of the knee and the distances from both cuffs to the knee joint significantly affect the maximum moment efficiency index. According to Fig. 4, when assisting the knee in flexion, the maximum moment efficiency index does not change much with the shank cuff moving closer to the knee (i.e., d_s decreases) or the flexion of

the knee (i.e., ϕ_k increases). However, when the upper leg cuff is within 0.1 m from the knee ($d_u \leq 0.1$ m), the maximum moment efficiency index decreases sharply with the upper leg cuff moving closer to the knee (i.e., d_u decreases). As shown in Fig. 5, when assisting the knee in extension, the maximum moment efficiency index increases with the shank cuff moving closer to the knee (i.e., d_s decreases), the upper leg cuff moving farther away from the knee (i.e., d_u increases), or the flexion of the knee (i.e., ϕ_k increases).

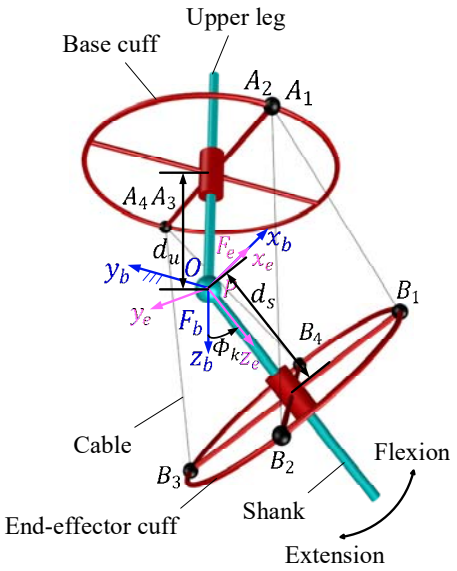

Fig. 3. Notations of a knee assisted by a three-DOF four-cable CDRD

TABLE I. POSITIONS OF ANCHOR POINTS (UNIT: M)

Anchor points	*Positions of Anchor points on the base (upper leg)*	*Positions of Anchor points on the end-effector (shank)*
1	$[0.1, 0.0, -d_u]^T$	$[0.0707, -0.0707, d_s]^T$
2	$[0.1, 0.0, -d_u]^T$	$[0.0707, 0.0707, d_s]^T$
3	$[-0.1, 0.0, -d_u]^T$	$[-0.0707, 0.0707, d_s]^T$
4	$[-0.1, 0.0, -d_u]^T$	$[-0.0707, -0.0707, d_s]^T$

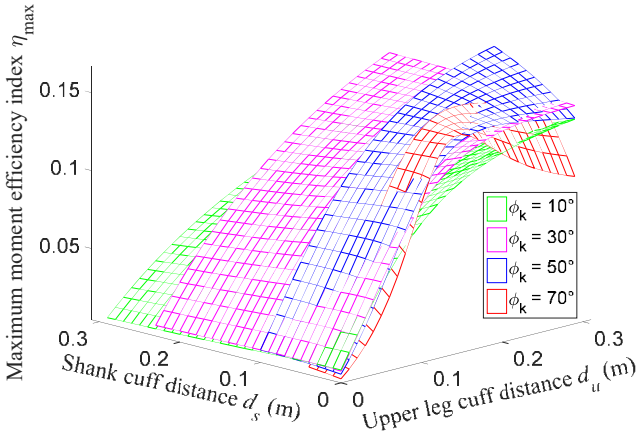

Fig. 4. The maximum moment efficiency index of the CDRD when assisting the flexion of the knee

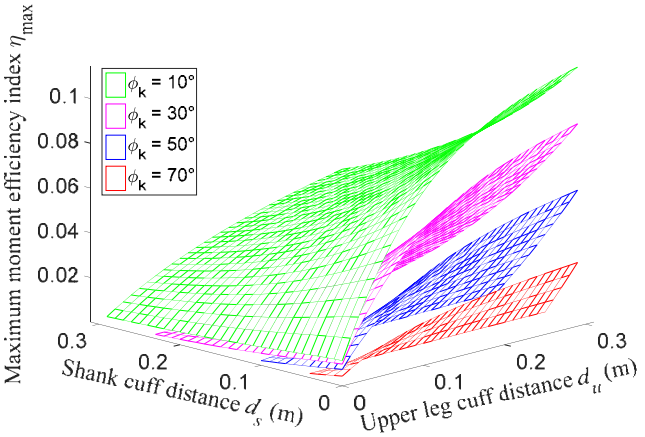

Fig. 5. The maximum moment efficiency index of the CDRD when assisting the extension of the knee

Based on Figs. 4 and 5, one can conclude that if the CDRD showed in Fig. 3 is used for knee rehabilitation or assistance, wearing the shank cuff close to the knee allows the CDRD to assist the knee with a large angle of the knee while wearing the upper leg cuff far away from the knee (up to about 0.15 m) can improve the moment efficiency of the CDRD. These findings on positioning the cuffs provide a cornerstone for further study (e.g., control and assistance strategies) of this CDRD.

V. CONCLUSION

In this paper, the joint force generated by a CDRD in assisting a human joint was analyzed. The kinematics and dynamics models of a general three-DOF human joint assisted by a three-DOF four-cable CDRD were established first. Then, the moment efficiency index was proposed to quantitatively evaluate the efficiency of a CDRD in providing assistant moment to a human joint. A case study of a knee with one DOF assisted by a three-DOF CDRD with four cables was conducted based on the moment efficiency index. The moment efficiency index proposed in this paper not only promotes safety of rehabilitation training, but also provides a guideline to for the design of CDRDs.

REFERENCES

[1] R. Morales, F. J. Badesa, N. García-Aracil, J. M. Sabater, and C. Pérez-Vidal, "Pneumatic robotic systems for upper limb rehabilitation," *Med. Biol. Eng. Comput.*, vol. 49, no. 10, p. 1145, 2011.

[2] R. Van Peppen, G. Kwakkel, B. Harmeling-van der Wel, B. Kollen, J. Hobbelen, and J. Buurke, "KNGF clinical practice guideline for physical therapy in patients with stroke. Review of the evidence," *Ned. Tijdschr. voor Fysiother.*, vol. 114, no. 5, 2004.

[3] P. Maciejasz, J. Eschweiler, K. Gerlach-Hahn, A. Jansen-Troy, and S. Leonhardt, "A survey on robotic devices for upper limb rehabilitation," *J. Neuroeng. Rehabil.*, vol. 11, no. 1, p. 3, 2014.

[4] N. Norouzi-Gheidari, P. S. Archambault, and J. Fung, "Effects of robot-assisted therapy on stroke rehabilitation in upper limbs: systematic review and meta-analysis of the literature," *J. Rehabil. Res. Dev.*, vol. 49, no. 4, p. 479, 2012.

[5] R. A. R. C. Gopura, D. S. V Bandara, K. Kiguchi, and G. K. I. Mann, "Developments in hardware systems of active upper-limb exoskeleton robots: A review," *Rob. Auton. Syst.*, vol. 75, pp. 203–220, 2016.

[6] J. Du and S. K. Agrawal, "Dynamic Modeling of Cable-Driven Parallel Manipulators With Distributed Mass Flexible Cables," *J. Vib. Acoust.*, vol. 137, no. 2, p. 21020, 2015.

[7] D. Mayhew, B. Bachrach, W. Z. Rymer, and R. F. Beer, "Development of the MACARM-a novel cable robot for upper limb neurorehabilitation," in *Rehabilitation Robotics, 2005. ICORR 2005.*

9th International Conference on, 2005, pp. 299–302.

[8] Y. Mao and S. K. Agrawal, "Design of a cable-driven arm exoskeleton (CAREX) for neural rehabilitation," *IEEE Trans. Robot.*, vol. 28, no. 4, pp. 922–931, 2012.

[9] X. Cui, W. Chen, J. Zhang, and J. Wang, "Note: Model-based identification method of a cable-driven wearable device for arm rehabilitation," *Rev. Sci. Instrum.*, vol. 86, no. 9, p. 096107, 2015.

[10] X. Jin, X. Cui, and S. K. Agrawal, "Design of a cable-driven active leg exoskeleton (c-alex) and gait training experiments with human subjects," in *Robotics and Automation (ICRA), 2015 IEEE International Conference on*, 2015, pp. 5578–5583.

[11] P. K. Jamwal, S. Xie, and K. C. Aw, "Kinematic design optimization of a parallel ankle rehabilitation robot using modified genetic algorithm," *Rob. Auton. Syst.*, vol. 57, no. 10, pp. 1018–1027, 2009.

[12] W. Chen, X. Cui, J. Zhang, and J. Wang, "A cable-driven wrist robotic rehabilitator using a novel torque-field controller for human motion training," *Rev. Sci. Instrum.*, vol. 86, no. 6, pp. 0–14, 2015.

[13] I. Galiana, F. L. Hammond, R. D. Howe, and M. B. Popovic, "Wearable soft robotic device for post-stroke shoulder rehabilitation: Identifying misalignments," in *Intelligent Robots and Systems (IROS), 2012 IEEE/RSJ International Conference on*, 2012, pp. 317–322.

[14] S. B. Kesner, L. Jentoft, F. L. Hammond, R. D. Howe, and M. Popovic, "Design considerations for an active soft orthotic system for shoulder rehabilitation," in *Engineering in Medicine and Biology Society, EMBC, 2011 Annual International Conference of the IEEE*, 2011, pp. 8130–8134.

[15] Y. Park, J. Santos, K. G. Galloway, E. C. Goldfield, and R. J. Wood, "A Soft Wearable Robotic Device for Active Knee Motions using Flat Pneumatic Artificial Muscles," pp. 4805–4810, 2014.

[16] Park，Yong-Lae, Chen，Bor-rong, N. O. P´erez-Arancibia, D. Young, L. Stirling, R. J. Wood, E. C. Goldfield, and R. Nagpal, "Design and control of a bio-inspired soft wearable robotic device for ankle – foot," vol. 016007.

[17] J.-M. Belda-Lois, S. Mena-del Horno, I. Bermejo-Bosch, J. C. Moreno, J. L. Pons, D. Farina, M. Iosa, M. Molinari, F. Tamburella, A. Ramos, A. Caria, T. Solis-Escalante, C. Brunner, and M. Rea, "Rehabilitation of gait after stroke: a review towards a top-down approach," *J. Neuroeng. Rehabil.*, vol. 8, no. 1, p. 66, 2011.

[18] Y. Mao and S. K. Agrawal, "Wearable Cable-driven Upper Arm Exoskeleton - Motion with Transmitted Joint Force and Moment Minimization," pp. 4334–4339, 2010.

[19] K. Ikuta, H. Ishii, and M. Nokata, "Safety evaluation method of design and control for human-care robots," *Int. J. Rob. Res.*, vol. 22, no. 5, pp. 281–297, 2003.

[20] S. K. Mustafa and S. K. Agrawal, "On the force-closure analysis of n-DOF cable-driven open chains based on reciprocal screw theory," *Robot. IEEE Trans.*, vol. 28, no. 1, pp. 22–31, 2012.

[21] X. Diao and O. Ma, "A method of verifying force-closure condition for general cable manipulators with seven cables," *Mech. Mach. Theory*, vol. 42, no. 12, pp. 1563–1576, 2007.

[22] M. R. Napolitano, *Aircraft dynamics: From modeling to simulation*. J. Wiley, 2012.

[23] R. F. Stengel, *Flight dynamics*. Princeton University Press, 2015.

[24] R. W. Beard and T. W. McLain, *Small unmanned aircraft: Theory and practice*. Princeton university press, 2012.

[25] L. Amezquita-Brooks, E. Liceaga-Castro, M. Gonzalez-Sanchez, O. Garcia-Salazar, and D. Martinez-Vazquez, "Towards a standard design model for quad-rotors: A review of current models, their accuracy and a novel simplified model," *Prog. Aerosp. Sci.*, 2017.

[26] E. Ottaviano and G. Castelli, "A study on the effects of cable mass and elasticity in cable-based parallel manipulators," *Rom. 18 Robot Des. Dyn. Control*, pp. 149–156, 2010.

[27] M. A. Khosravi and H. D. Taghirad, "Robust PID control of fully-constrained cable driven parallel robots," *Mechatronics*, vol. 24, no. 2, pp. 87–97, 2014.

[28] O. Ma and X. Diao, "Dynamics analysis of a cable-driven parallel manipulator for hardware-in-the-loop dynamic simulation," in *Advanced Intelligent Mechatronics. Proceedings, 2005 IEEE/ASME International Conference on*, 2005, pp. 837–842.

[29] D. Q. Nguyen and M. Gouttefarde, "Stiffness matrix of 6-dof cable-driven parallel robots and its homogenization," in *Advances in Robot Kinematics*, Springer, 2014, pp. 181–191.

[30] H. Xiong and X. Diao, "The effect of cable tensions on the stiffness of cable-driven parallel manipulators," in *Advanced Intelligent Mechatronics (AIM), 2017 IEEE International Conference on*, 2017, pp. 1185–1190.

[31] H. Xiong and X. Diao, "Cable tension control of cable-driven parallel manipulators with position-controlling actuators," in *2017 IEEE International Conference on Robotics and Biomimetics (ROBIO)*, 2017, pp. 1763–1768.